

# Dynein harnesses active fluctuations of microtubules for faster movement

Yasin Ezber<sup>1</sup>, Vladislav Belyy<sup>2</sup>, Sinan Can<sup>1</sup> and Ahmet Yildiz 1,2,3\*

The cytoskeleton forms a dynamic network that generates fluctuations larger than thermal agitation of the cytoplasm<sup>1</sup>. Here, we tested whether dynein, a minus-end-directed microtubule (MT) motor2, can harness energy from these fluctuations using optical trapping in vitro. We show that dynein forms an asymmetric slip bond with MTs, where its detachment rate increases more slowly under hindering forces than assisting forces. This asymmetry enables dynein to generate unidirectional motility towards the minus-end from force fluctuations. Consistent with our model, oscillatory forces exerted by the trap drive dynein stepping without net force and ATP. Dynein is capable of ratcheting towards the minus-end, even when the net force is in the plus-end direction. With ATP, force oscillations increase the velocity and stall force of dynein as it transports cargos and glides MTs. Therefore, dynein is a mechanical ratchet that rectifies cytoskeletal fluctuations to move faster and resists higher forces along MTs.

The cellular interior is highly dynamic and far from equilibrium. The mechanical properties of the cytoplasm are dominated by the dynamics of cytoskeletal filaments, microtubules (MTs) and actin, which harness energy from nucleotide triphosphate hydrolysis. These polar filaments rapidly polymerize and depolymerize, providing a continuous supply of mechanical energy to the cell. Molecular motors (actin-associated myosins and MT-associated kinesins and dyneins) also use energy from ATP hydrolysis to generate force and mechanical work along these tracks. Collectively, the cytoskeleton forms an active network. Forces generated by filament polymerization and motors control the flow of cytoplasmic streaming and drive the motion of large objects in the cytoplasmic streaming and drive the motion of large objects in the cytoplasmic, in principle, be harnessed by molecular machines to perform mechanical work.

Although the roles of molecular motors in motility, contractility and self-organization of cytoskeletal networks have been studied in detail, little is known about how active fluctuations of the cytoskeleton affect the mechanics and cellular function of cytoskeletal motors and non-motor proteins. MT-associated proteins (MAPs) such as NuMA and EB1 exhibit asymmetric friction when they crosslink a pair of actively moving MTs, and this may be a viable strategy for these proteins to diffuse towards one end during MT growth and shrinkage<sup>4</sup>. The actin-binding proteins, vinculin and cadherincatenin, form a force-dependent catch bond when pulled towards the pointed end of the actin, which may reinforce cell adhesion and maintain front–rear asymmetry in migrating cells<sup>5,6</sup>. Similarly, myosin II and kinesin-8 motors diffuse at different speeds towards the plus- and minus-ends of actin and MTs under load<sup>7,8</sup>.

It remains unclear whether processive motors can harness energy from cytoskeletal fluctuations for faster stepping along their tracks. Optical trapping studies have revealed that dynein (Fig. 1a), a motor

protein responsible for nearly all motility and force generation functions towards the MT minus-end, rapidly releases from MTs and moves faster when pulled forward, while resisting backward movement when pulled towards the plus-end<sup>9-12</sup>. This asymmetry has been proposed to play a role in the interhead coordination of dynein motility<sup>10,13,14</sup>, as well as tight anchoring of dynein to MTs under high tension<sup>15</sup>.

To test dynein's ability to harness energy from cytoskeletal fluctuations, we first characterized the force-dependent kinetics of the dynein-MT bond. Previous studies proposed that dynein-MT is a slip-ideal<sup>12</sup>, ideal<sup>11</sup> or catch<sup>15</sup> bond, predicting that the release rate remains constant or decreases under high hindering forces (Extended Data Fig. 1a). These models could not be distinguished because of the small changes in the velocity and MT release rate of dynein under low (1-5pN) hindering forces (Extended Data Fig. 1a). To address this, we measured the MT dwell time of single Saccharomyces cerevisiae cytoplasmic dynein ('dynein' hereafter) monomers<sup>16</sup> under a wider range of forces (1-14pN), using an optical trap<sup>10,17</sup> (Fig. 1b and Extended Data Fig. 2). The dwell time distributions fit well to a double exponential decay. The MT release rate was interpreted as the slow rate of the fit, whereas the fast rate probably represents weak interactions between dynein and MT (Extended Data Fig. 1b-d). Consistent with previous studies<sup>10,12</sup>, we observed that the release rate rapidly increases when dynein was pulled toward the MT minus-end (assisting), and release was slow at low hindering forces (1-4 pN) in the absence of ATP. However, we clearly detected an increase in MT release rate at higher hindering forces (6-14 pN), albeit less drastically than release under the forward pull of the trap (Fig. 1c). These results show that dynein forms an asymmetric slip bond with an MT. The force-detachment kinetics of dynein from MT can be described by a model<sup>8</sup> based on Arrhenius theory (see Supplementary Information). In the absence of force and nucleotide, forward ( $k_{\text{minus}}$ ) and backward ( $k_{\text{plus}}$ ) release rates are equal:

$$k_{\text{minus}} = k_{\text{plus}} = k_0^{\text{apo}} \propto e^{-\Delta G_0/k_{\text{B}}T}$$
 (1)

where  $k_0^{\rm apo}$  is the release rate and  $\Delta G_0$  is the energy barrier in the absence of force and nucleotide,  $k_{\rm B}$  is the Boltzmann constant and T is the absolute temperature (Fig. 1d(i)). An external force (F, positive forces are in the plus-end direction) biases the potential landscape and increases the release rate towards the direction in which the motor is pulled from the MT (Fig. 1d(ii)):

$$k_{\text{minus}} = k_0^{\text{apo}} e^{-F(\frac{\delta}{2} + A)/k_B T}, k_{\text{plus}} = k_0^{\text{apo}} e^{F(\frac{\delta}{2} - A)/k_B T}$$
 (2)

where A is the asymmetric distance that biases the energy barrier for release from the MT and  $\delta$  is the barrier width (Fig. 1d(ii)). The total release rate ( $k_{\text{total}}$ ) is given by:

Physics Department, University of California, Berkeley, CA, USA. Biophysics Graduate Group, University of California, Berkeley, CA, USA.

<sup>&</sup>lt;sup>3</sup>The Department of Molecular and Cell Biology, University of California, Berkeley, CA, USA. \*e-mail: yildiz@berkeley.edu

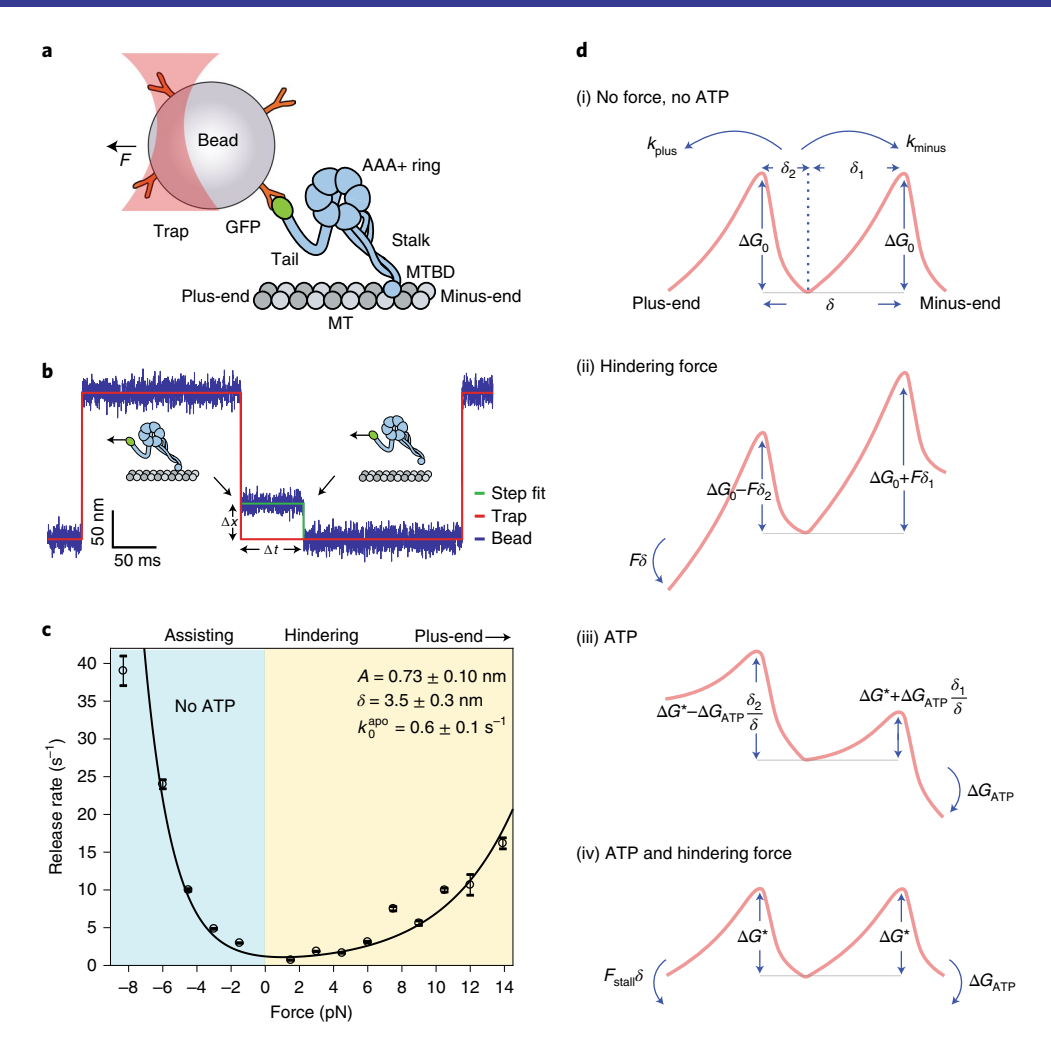


**Fig. 1** Dynein forms an asymmetric slip bond with an MT. a, Schematic of a dynein motor domain. The dynein heavy chain has a catalytic AAA+ ring, which connects to the MT binding domain (MTBD) through a coiled-coil stalk. Dynein was attached to an 860-nm-diameter polystyrene bead from its tail using the green fluorescent protein (GFP)-antibody linkage and trapped with a focused laser beam (not to scale). **b**, Measuring the force-induced release of dynein monomers from MTs. Inset: a trapped bead coated with monomeric dynein is oscillated between two positions 200 nm apart. When a dynein monomer binds to the MT, the bead does not follow the trap to its next position (black arrows). A constant force is applied due to trap-bead separation (Δx) until dynein releases from the MT (Δt). **c**, The release rates of dynein monomers from MT under force are calculated from an exponential decay fit to the dwell time histograms (error bars indicate ± standard error (s.e.); n = 270, 243, 479, 407, 385, 354, 487, 461, 380, 260, 208, 325, 137 and 325, from left to right; Extended Data Fig 1). The solid curve represents a fit to equation (3). Errors in the derived parameters are s.e. of the fit. **d**, The model for the asymmetric potential landscape of dynein along an MT in the presence and absence of a nucleotide and external force ( $\delta_{1,2} = \delta/2 \pm A$ ). The energy barrier in the presence of ATP ( $\Delta G^*$ ) is lower than the apo condition ( $\Delta G_{0}$ ) (i). Work done by the hindering force ( $F\delta$ ) shears the energy landscape towards the plus-end (ii), while the free energy of ATP hydrolysis ( $\Delta G_{ATP}$ ) shears it towards the minus-end (iii). At  $F_{stall} = -\Delta G_{ATP}/\delta$ , the motor comes to a stall because the negative work done by hindering force is equal to the positive work done by ATP hydrolysis (iv).

$$k_{\text{total}} = k_{\text{minus}} + k_{\text{plus}} = 2k_0^{\text{apo}} e^{-\frac{FA}{k_BT}} \cosh\left(\frac{F\delta}{2k_BT}\right)$$
 (3)

The fit of the force-dependent release rate to equation (3) reveals that A of dynein  $(0.73\pm0.10\,\mathrm{nm},\mathrm{Fig.\ 1c})$  is higher than the previously reported values for kinesin-8 $^8$ , NuMA and EB1 $^4$ , suggesting that dynein is a stronger ratchet than these proteins. We note that  $\delta$  (3.4±0.3 nm) represents the distance over which the external force acts on a dynein monomer to release it from MT and it is shorter than the distance between adjacent tubulin binding sites (8.2 nm). Due to the vertical forces inherent to the single bead trapping assay<sup>18</sup>, we anticipate that  $k_0^{\mathrm{apo}}$  of the motor is lower than the  $0.6\pm0.1\,\mathrm{s}^{-1}$  we measured and that dynein exhibits even greater asymmetry in the absence of vertical forces.

To determine how force affects the motility of the dynein dimers, we applied constant forces to beads transported by single full-length

dynein<sup>16</sup> (Fig. 2a). In the absence of ATP, dynein was immobile in the absence of force and moved processively towards the direction in which it was being pulled by the optical trap<sup>9</sup>. Consistent with its asymmetric force-dependent detachment from MT, dynein moved faster towards the minus-end compared to the plus-end under the same magnitude of force (Fig. 2b)<sup>9,11,19</sup>. The average velocity (*V*, positive velocities are in the minus-end direction) at a given force is given by

$$V(F) = k_{\text{total}}(F)d(F) \tag{4}$$

where d(F) is the average step size of dynein in the absence of ATP. We measured d(F) from the step analysis of individual trajectories under constant load (Extended Data Fig. 3). The fit of experimentally measured V(F)/d(F) values to equation (3) (Extended Data Fig 3d) revealed similar  $k_0^{\rm apo}$ , A and  $\delta$  values,

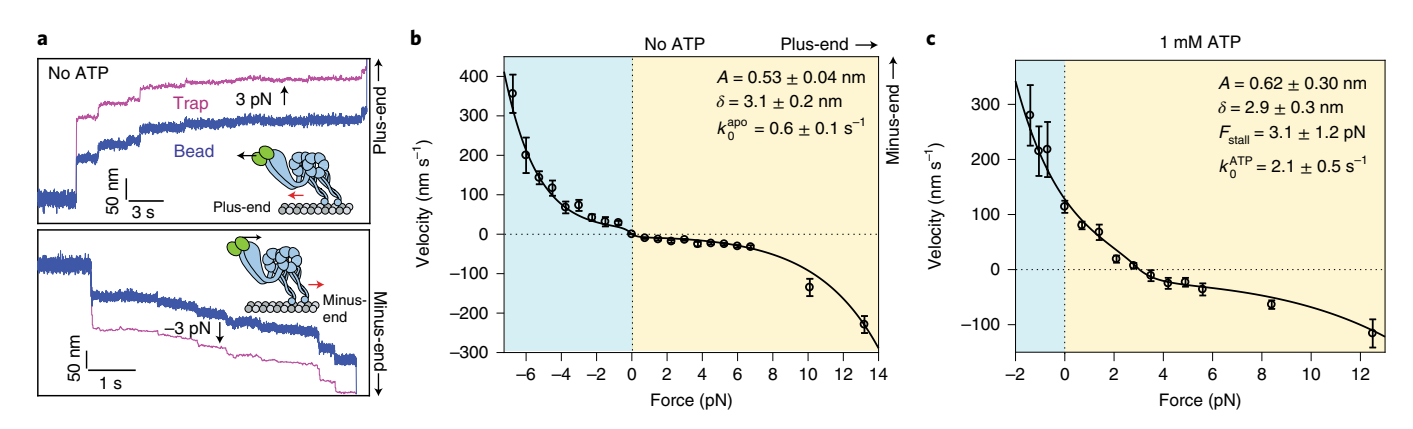


**Fig. 2** | **Dynein responds asymmetrically to assisting and hindering forces. a**, Representative position-time graph of a dynein motor under constant 3 pN hindering (top) and assisting (bottom) forces. Insets: dynein moves (red arrows) towards the direction of the applied force (black arrow). **b**, *F-V* relationship of dynein in the absence of ATP (mean±s.e.m.; from left to right n=51, 50, 59, 53, 41, 35, 48, 46, 43, 54, 62, 47, 82, 68, 56, 92, 85, 44, 45 and 78 from three technical replicates). **c**, *F-V* relationship of dynein in 1mM ATP (mean±s.e.m.; from left to right n=38, 36, 48, 78, 42, 56, 58, 47, 39, 35, 35, 48, 43 and 42 from three technical replicates). In **b** and **c**, the solid curves represent a fit to equations (3) and (5), respectively (see Supplementary Information). Errors of the derived parameters are s.e. of the fit.

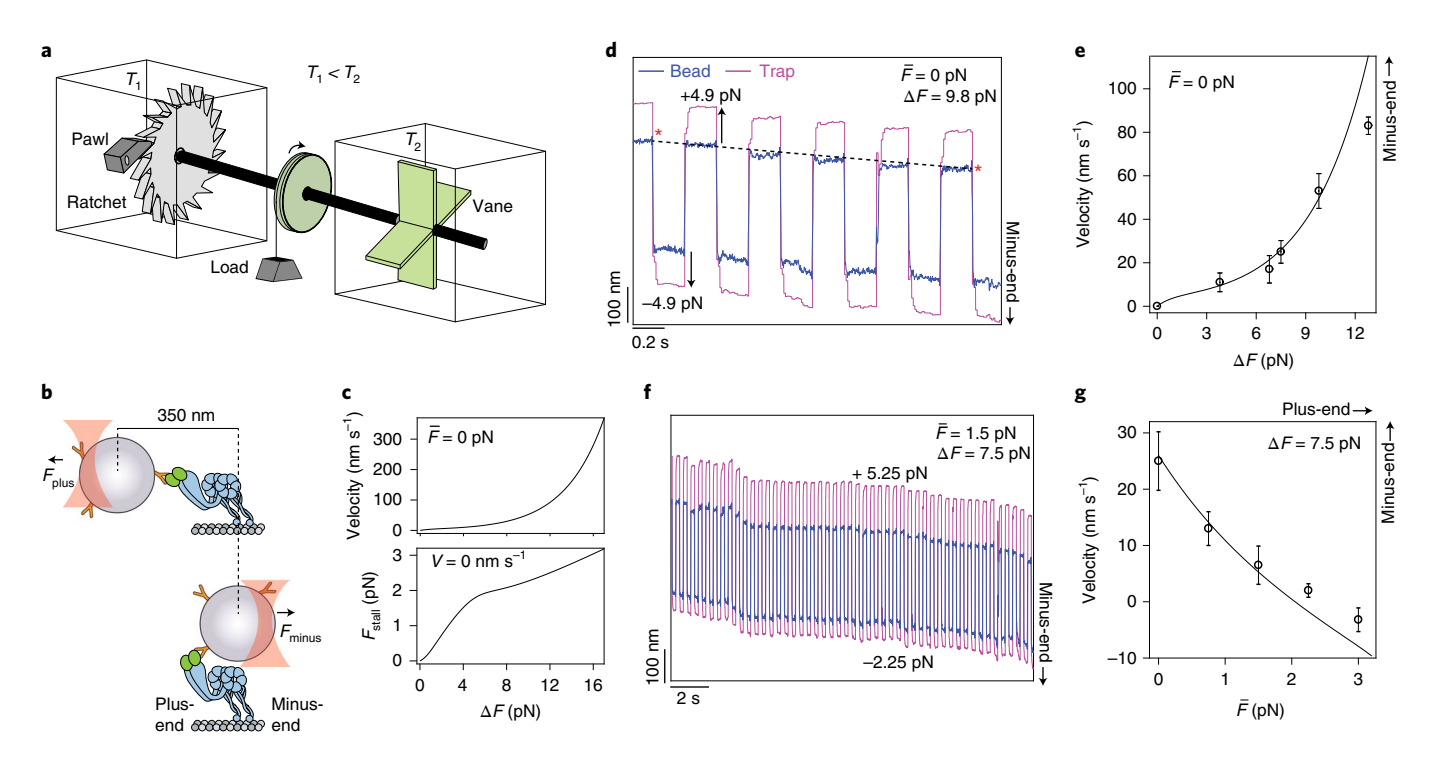


**Fig. 3** | Force oscillations drive minus-end-directed motility of dynein without ATP. **a**, Feynman's microscopic ratchet device. Two chambers are maintained at temperatures  $T_1$  and  $T_2$ . Thermal fluctuations in the right chamber drive the shaft. The ratchet generates net clockwise rotation and lifts the load if  $T_2 > T_1$ . **b**, Dynein is driven by back-and-forth oscillations of the optically trapped bead, which increase the local effective temperature above that of the environment. Due to the rotational freedom of the bead, the trap freely moves 350 nm between the assisting and hindering directions before applying a significant force on dynein. **c**, The velocity and stall force of dynein under force oscillations are estimated from the F-V curve in Fig. 2b. **d**, A dynein-driven bead oscillating  $\pm 4.9$  pN in a square-wave pattern at 2.5 Hz exhibits motility towards the MT minus-end. The velocity is calculated from the ratio of the net displacement of the bead (black dashed line) to elapsed time (red asterisks). **e**, The minus-end-directed velocity of dynein-driven beads increases with  $\Delta F$  (mean  $\pm$  s.d.; from left to right n = 32, 35, 25, 39 and 42 from three technical replicates). **f**, Example trajectory of a dynein-driven bead oscillating with 5.25 pN hindering and -2.25 pN assisting forces at 2.5 Hz. **g**, The velocity of dynein-driven beads decreases with the increase in the average hindering force on the bead (mean  $\pm$  s.d.; from left to right n = 25, 23, 29, 28 and 25 from three technical replicates). In **e** and **g**, black curves represent the estimated velocities from the F-V curve in Fig. 2b.

estimated from the force-dependent release rates of monomeric dynein (Fig. 1c).

We next determined how force affects dynein velocity in saturating (1 mM) ATP. Similar to the results in ref. 9, we observed

that dynein responds asymmetrically to load, and moves processively backward under high resistive forces (Fig.  $2c)^{9,11}$ . However, we observed dynein to move at higher velocities  $(114\pm11\,\mathrm{nm\,s^{-1}}\ (\pm\mathrm{s.e.m.}))$  in unloaded conditions<sup>16</sup> and the velocity increased

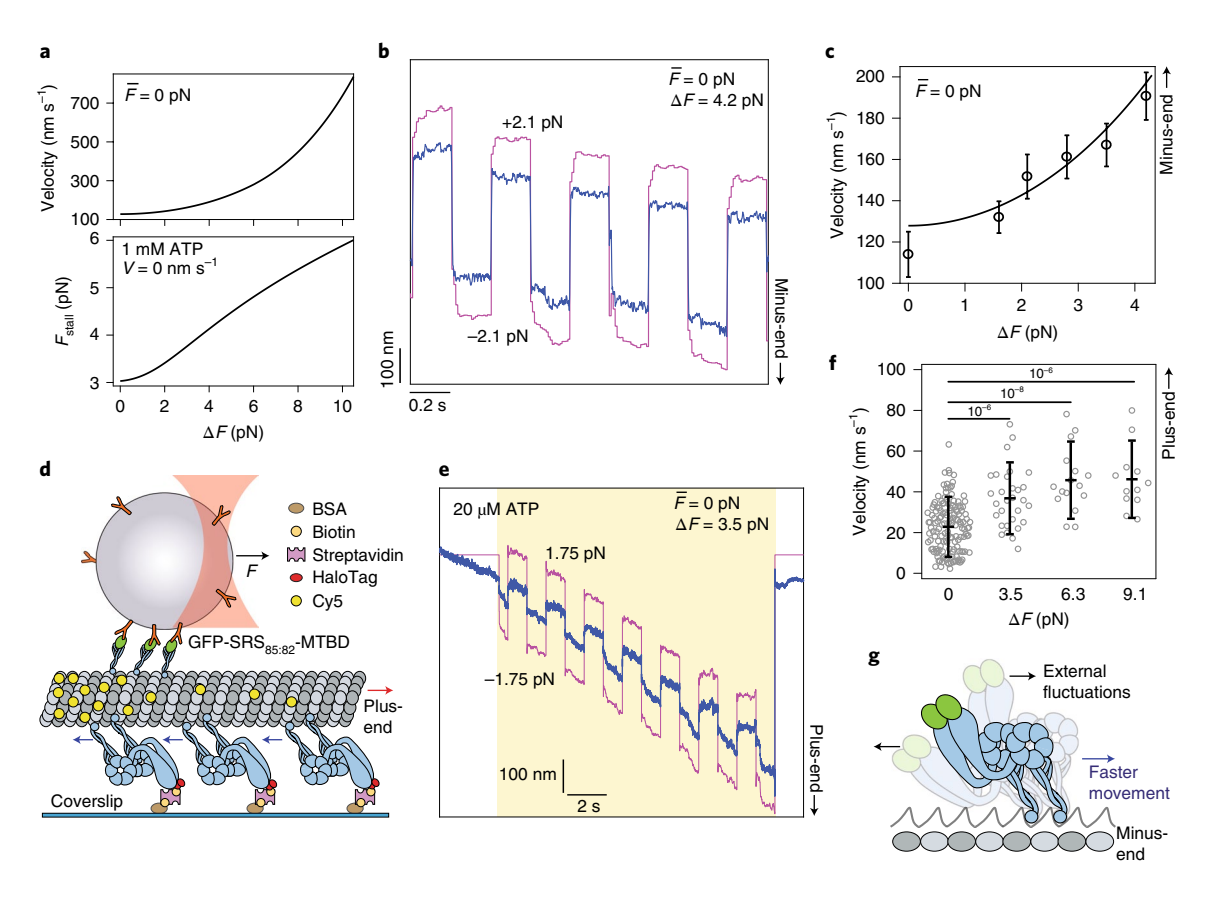


**Fig. 4 | Force oscillations increase cargo transport and MT gliding velocity of dynein in the presence of ATP. a**, The velocity and stall force of dynein under force oscillations are estimated from the *F-V* curve in Fig. 2c. **b**, Example trajectory of a dynein-driven bead oscillating  $\pm 2.1$  pN at 2.5 Hz. **c**, The velocity of dynein-driven beads increases with the increase in Δ*F* on the bead (mean  $\pm$  s.d.; n = 78, 42, 35, 28, 30 and 21 from left to right from three technical replicates). The black curve shows the estimated velocities in **a**. **d**, Schematic of the optical trapping assay for the MT oscillations. Dyneins were fixed on the glass surface from their tail through a biotin–streptavidin linkage. MTs glide with their plus-end in the lead (red arrow) due to the minus-end-directed motility of surface-immobilized dyneins (blue arrow). The trapped bead was tightly attached to a gliding MT on the surface and oscillated back and forth at 1Hz. **e**, Example trajectory of a gliding MT oscillating  $\pm$ 1.75 pN at 1Hz in 20 μM ATP. The yellow shaded region represents the duration the force feedback was engaged for trap oscillations. **f**, MT gliding velocity increases versus the magnitude of force fluctuations. Data at 0 pN were obtained from fluorescence experiments. The centre line and edges represent mean and s.d., respectively. *P* values are calculated from Welch's *t*-test (n = 144, 30, 16 and 12 from left to right). **g**, Due to the asymmetric force-detachment kinetics, dynein ratchets towards the minus-end of MTs under external fluctuations.

rapidly under forward load. In addition, we did not see evidence of a non-advancing stepping mode<sup>9</sup>, in which the motor takes consecutive forward and backward steps at the same position on an MT under load. These disparities may be related to differences in the assay conditions and the calibration of the force response of the optical trap.

To determine how energy from nucleotide hydrolysis biases the potential landscape towards the minus-end (Fig. 1d(iii)), we fit the F-V measurements to

$$V(F) = 2d(F)k_0^{\text{ATP}} e^{-\frac{(F - F_{\text{stall}})A}{k_B T}} \cosh\left(\frac{(F - F_{\text{stall}})\delta}{2k_B T}\right)$$
 (5)

where  $k_0^{\rm ATP}$  is the release rate in the absence of force, and  $F_{\rm stall}$  is the hindering force at which  $k_{\rm minus}\!=\!k_{\rm plus}$  (Fig. 1d(iv)). The average step size in ATP at a given force (d(F)) was measured from individual trajectories under constant load (Extended Data Fig. 4). The fit revealed A and  $\delta$  values similar to those for the no nucleotide condition (Extended Data Fig. 4d).  $F_{\rm stall}$  (3.1 pN) is consistent with earlier measurements in fixed trap assays and lower than the 7 pN stall force reported in ref. (Fig. 2c). Notably,  $k_0^{\rm ATP}$  is approximately fourfold higher than  $k_0^{\rm apo}$ , which might result from switching of dynein

from strongly bound to weakly bound states during the nucleotide hydrolysis cycle.

To test whether this asymmetric F–V relationship enables dynein to harness energy from cytoskeletal oscillations, we designed an experiment analogous to Feynman's hypothetical 'ratchet and pawl' device<sup>20</sup>, in which a microscopic ratchet generates work from random fluctuations that occur at an effective temperature higher than the ambient temperature (Fig. 3a). We increased the effective temperature, but not the actual temperature, of a single dynein's local environment by oscillating the optically trapped bead (Fig. 3b,c). We first checked whether force fluctuations can drive unidirectional motility without ATP and the average force on the bead  $(\bar{F} = (F_{\text{plus}} + F_{\text{minus}})/2)$ . The magnitude of force oscillations  $(\Delta F = F_{\text{plus}} - F_{\text{minus}})$  was increased from 0 pN to 13 pN, while  $\bar{F}$ was kept at 0 pN (Fig. 3d,e and Extended Data Fig. 5). Consistent with our prediction, dynein processively moved towards the minusend when subjected to force oscillations in a square-wave pattern and the velocity increased with  $\Delta F$  (Fig. 3e). The  $\Delta F$ –V relationship is consistent with the average velocities of dynein under  $F_{\text{plus}}$  and  $F_{\text{minus}}$  (Fig. 2b,e).

To test the effectiveness of dynein's ratcheting along MTs in the absence of ATP, we biased  $\bar{F}$  from 0 pN to 3 pN towards the

plus-end while keeping  $\Delta F$  constant (7.5 pN). Remarkably, dynein was able to move towards the minus-end even though it was pulled more strongly towards the plus-end. The motor stalled at  $\bar{F}=2$  pN and moved backwards under higher hindering loads (Fig. 3f,g and Extended Data Fig. 5). We also observed the mammalian dynein-dynactin–BicD2N (DDB) complex<sup>21</sup> to move processively towards the MT minus-end under force fluctuations in the absence of ATP and net force (Extended Data Fig. 6), suggesting that ratcheting is a general property of dynein motors.

We next tested our prediction that dynein's ratcheting along MTs increases the velocity and stall force under physiological ATP concentrations (Fig. 4a). We measured the velocity of dynein-driven beads subjected to force oscillations in 1 mM ATP (Fig. 4b). At  $\overline{F}=0$  pN, application of  $\Delta F$  up to 4.2 pN increased the velocity by 67% (190±11 nm s<sup>-1</sup>, Fig. 4c), demonstrating that dynein moves faster by harnessing the energy of force fluctuations under saturating ATP.

In cells, dynein motors also anchor onto large organelles or the plasma membrane and pull the MTs. To test whether oscillations of the MT network affect the MT sliding activity via multiple dyneins, we oscillated beads attached to MTs as they were glided by surface-immobilized dyneins (Fig. 4d). To initiate force oscillations before the beads escaped the trap, we lowered the gliding velocity under no force to  $23\pm2\,\mathrm{nm\,s^{-1}}$  (mean  $\pm$  s.e.m.) by reducing the ATP concentration to  $20\,\mu\mathrm{M}$ . The trajectories revealed that assisting forces significantly increased the gliding velocity whereas hindering forces caused a modest slowdown of MT gliding (Fig. 4e). In the absence of a net force, the application of  $\Delta F$  up to 6.3 pN caused a twofold increase in gliding speed (Fig. 4f), demonstrating that the oscillation of MTs leads to faster filament sliding activity of dynein motors.

Collectively, our results show that dynein forms an asymmetric slip bond with an MT, which enables this motor to harness energy from cytoskeletal fluctuations (Fig. 4g). Unlike myosin V, which functions as a reverse ratchet<sup>22</sup>, dynein is a forward ratchet that favours faster movement when pulled towards its natural direction of motion. Therefore, fluctuations increase the speed of dynein motility and the ability of the motor to resist hindering forces, resulting in higher power output (Extended Data Fig. 7).

It is possible that ratcheting along MTs may assist dynein to perform its cellular functions. Dynein carries organelles and vesicles towards the nucleus of interphase cells and drives retrograde transport towards the cell body in neurons<sup>2</sup>. Dyneins also generate periodic oscillations of MTs on millisecond to minute timescales<sup>23</sup>. During asymmetric cell division, the entire mitotic spindle undergoes periodic oscillations due to antagonistic force generation of cortical dyneins, and this is attributed to force-dependent detachment of dynein from an MT<sup>24,25</sup>. Ratcheting may enable dyneins to move towards the minus-end at faster speeds and increase tension for proper positioning of the spindle<sup>26</sup>. Similarly, the beating of motile cilia is powered by antagonistic forces generated by axonemal dyneins on opposite sides of an axoneme. Active oscillations of the parallel bundle of MTs may increase the MT sliding velocity of axonemal dyneins (Fig. 4) and the frequency of ciliary beating<sup>27,28</sup>. Our oscillating trap assay can be combined with efforts regarding in vitro reconstitution of the mitotic spindle<sup>29</sup> and cilia-like beating of MT bundles<sup>30</sup> for testing these ideas.

# Online content

Any methods, additional references, Nature Research reporting summaries, source data, extended data, supplementary information, acknowledgements, peer review information; details of author contributions and competing interests; and statements of data and code availability are available at <a href="https://doi.org/10.1038/s41567-019-0757-4">https://doi.org/10.1038/s41567-019-0757-4</a>.

Received: 23 February 2019; Accepted: 15 November 2019; Published online: 20 January 2020

## References

- Mizuno, D., Tardin, C., Schmidt, C. F. & Mackintosh, F. C. Nonequilibrium mechanics of active cytoskeletal networks. *Science* 315, 370–373 (2007).
- Roberts, A. J., Kon, T., Knight, P. J., Sutoh, K. & Burgess, S. A. Functions and mechanics of dynein motor proteins. *Nat. Rev. Mol. Cell Biol.* 14, 713–726 (2013).
- Fakhri, N. et al. High-resolution mapping of intracellular fluctuations using carbon nanotubes. Science 344, 1031–1035 (2014).
- Forth, S., Hsia, K. C., Shimamoto, Y. & Kapoor, T. M. Asymmetric friction of nonmotor MAPs can lead to their directional motion in active microtubule networks. *Cell* 157, 420–432 (2014).
- Buckley, C. D. et al. Cell adhesion. The minimal cadherin-catenin complex binds to actin filaments under force. Science 346, 1254211 (2014).
- Huang, D. L., Bax, N. A., Buckley, C. D., Weis, W. I. & Dunn, A. R. Vinculin forms a directionally asymmetric catch bond with F-actin. *Science* 357, 703–706 (2017).
- Guo, B. & Guilford, W. H. Mechanics of actomyosin bonds in different nucleotide states are tuned to muscle contraction. *Proc. Natl Acad. Sci. USA* 103, 9844–9849 (2006).
- Bormuth, V., Varga, V., Howard, J. & Schaffer, E. Protein friction limits diffusive and directed movements of kinesin motors on microtubules. *Science* 325, 870–873 (2009).
- 9. Gennerich, A., Carter, A. P., Reck-Peterson, S. L. & Vale, R. D. Force-induced bidirectional stepping of cytoplasmic dynein. *Cell* 131, 952–965 (2007).
- Cleary, F. B. et al. Tension on the linker gates the ATP-dependent release of dynein from microtubules. Nat. Commun. 5, 4587 (2014).
- Belyy, V., Hendel, N. L., Chien, A. & Yildiz, A. Cytoplasmic dynein transports cargos via load-sharing between the heads. *Nat. Commun.* 5, 5544 (2014).
- Nicholas, M. P. et al. Cytoplasmic dynein regulates its attachment to microtubules via nucleotide state-switched mechanosensing at multiple AAA domains. Proc. Natl Acad. Sci. USA 112, 6371–6376 (2015).
- DeWitt, M. A., Chang, A. Y., Combs, P. A. & Yildiz, A. Cytoplasmic dynein moves through uncoordinated stepping of the AAA+ ring domains. *Science* 335, 221–225 (2012).
- 14. Qiu, W. et al. Dynein achieves processive motion using both stochastic and coordinated stepping. *Nat. Struct. Mol. Biol* **19**, 193–200 (2012).
- Rai, A. K., Rai, A., Ramaiya, A. J., Jha, R. & Mallik, R. Molecular adaptations allow dynein to generate large collective forces inside cells. *Cell* 152, 172–182 (2013).
- Reck-Peterson, S. L. et al. Single-molecule analysis of dynein processivity and stepping behavior. Cell 126, 335–348 (2006).
- Dogan, M. Y., Can, S., Cleary, F. B., Purde, V. & Yildiz, A. Kinesin's front head is gated by the backward orientation of its neck linker. *Cell Rep.* 10, 1967–1973 (2015).
- Khataee, H. & Howard, J. Force generated by two kinesin motors depends on the load direction and intermolecular coupling. *Phys. Rev. Lett.* 122, 188101 (2019).
- Can, S., Lacey, S., Gur, M., Carter, A. P. & Yildiz, A. Directionality of dynein is controlled by the angle and length of its stalk. *Nature* 566, 407–410 (2019).
- Feynman, R. P., Leighton, R. B. & Sands, M. The Feynman Lectures on Physics, Vol. I: The New Millennium Edition: Mainly Mechanics, Radiation, and Heat Vol. 1 (Basic Books, 2011).
- Belyy, V. et al. The mammalian dynein-dynactin complex is a strong opponent to kinesin in a tug-of-war competition. *Nat. Cell Biol.* 18, 1018–1024 (2016).
- Gebhardt, J. C., Clemen, A. E., Jaud, J. & Rief, M. Myosin-V is a mechanical ratchet. Proc. Natl Acad. Sci. USA 103, 8680–8685 (2006).
- Campas, O. & Sens, P. Chromosome oscillations in mitosis. *Phys. Rev. Lett.* 97, 128102 (2006).
- Pecreaux, J. et al. Spindle oscillations during asymmetric cell division require a threshold number of active cortical force generators. *Curr. Biol.* 16, 2111–2122 (2006).
- Yang, G. et al. Architectural dynamics of the meiotic spindle revealed by single-fluorophore imaging. Nat. Cell Biol. 9, 1233–1242 (2007).
- Gaetz, J. & Kapoor, T. M. Dynein/dynactin regulate metaphase spindle length by targeting depolymerizing activities to spindle poles. J. Cell Biol. 166, 465–471 (2004).
- Shingyoji, C., Higuchi, H., Yoshimura, M., Katayama, E. & Yanagida, T. Dynein arms are oscillating force generators. *Nature* 393, 711–714 (1998).
- Lin, J. & Nicastro, D. Asymmetric distribution and spatial switching of dynein activity generates ciliary motility. Science 360, eaar1968 (2018).
- Laan, L. et al. Cortical dynein controls microtubule dynamics to generate pulling forces that position microtubule asters. Cell 148, 502–514 (2012).
- Sanchez, T., Welch, D., Nicastro, D. & Dogic, Z. Cilia-like beating of active microtubule bundles. *Science* 333, 456–459 (2011).

**Publisher's note** Springer Nature remains neutral with regard to jurisdictional claims in published maps and institutional affiliations.

© The Author(s), under exclusive licence to Springer Nature Limited 2020

## Methods

Protein purification and labelling. Full-length S. cerevisiae dynein was tagged with GFP at its N terminus and a HaloTag (DHA) at its C terminus and expressed under the native promoter<sup>16</sup>. To construct monomeric dynein, the 5' end of the dynein gene encoding the tail was deleted, leaving amino acids 1219-4093 with a predicted molecular weight of 331 kDa. The construct was tagged with GFP at its N terminus and DHA at its C terminus and expressed under a galactose promoter (GFP-Dyn331kD-DHA)16. For MT gliding assays, a GST dimer of tail-truncated dynein was tagged with DHA at the N terminus (DHA-GST-Dyn<sub>33kD</sub>)<sup>16</sup>. These constructs were purified from S. cerevisiae cultures by incubating the cell lysate with immunoglobulin-G (IgG) beads (GE Healthcare) and eluting the protein from beads using ZZ-TEV cleavage, as described previously<sup>16</sup>. The motor was labelled with 10 µM tetramethylrhodamine (TMR)- or biotin-alkyl chloride (a HaloTag ligand) at the DHA tag for an additional 1 h at 4 °C before cleaving the protein from the IgG beads. For DNA-tethered optical trapping experiments, a 74 bp doublestranded DNA tether was labelled with biotin at one end and alkyl chloride-NHS at the opposite end, and excess ligand was removed using ethanol precipitation at 4°C, as previously described11. DNA tether (10 μM) was incubated with monomeric dynein for an additional 1 h at 4°C before cleaving the protein from the IgG beads.

The constructs that express a phi mutant of human dynein (SNAP-DYNC1H1<sub>E1518K/R1567K</sub>) in a pACEBac1 vector backbone³¹¹, the pDyn2 plasmid that contains genes from IC2C, LIC2, TCTEX1, LC8 and ROBL1, and mouse BICD2–400-GFP (BicD2N-GFP) in a pOmniBac vector backbone were provided by A.P. Carter³²². Human dynein and BICD2N constructs contain a 6xHis-ZZ tag followed by a tobacco etch virus (TEV) protease cleavage site for protein purification. The proteins were expressed using the baculovirus insect cell system, and purified using TEV cleavage from IgG beads, as described previously³³. Dynactin was purified from pig brain using the large-scale SP-Sepharose and MonoQ ion-exchange chromatography³⁴. The 6xHis-tagged GFP-SRS<sub>8582</sub>-MTBD construct was expressed in *Escherichia coli* and purified using nickel-nitrilotriacetic affinity purification, as previously described³⁵. Purified protein was aliquoted and flash-frozen in liquid nitrogen. Protein purity was confirmed with gel electrophoresis and the concentration was measured using the QuickStart Bradford kit (BioRad).

Coating beads with anti-GFP antibodies. Carboxyl latex beads (860 nm in diameter, Life Technologies) were coated with custom-made rabbit polyclonal anti-GFP antibodies (Covance). A 200 µl volume of beads was resuspended three times in activation buffer (10 mM MES (2-(N-morpholino)ethanesulfonic acid) pH6.0, 100 mM NaCl) after spinning down at 8,000 r.p.m. for 3 min. EDC (1-ethyl-3-(3-dimethylaminopropyl)carbodiimide) (1 mg) and 1 mg of S-NHS (N-hydroxysulfosuccinimide) were dissolved in 1 ml and 2 ml DMF (dimethylformamide), respectively, and 20 µl of dissolved EDC and 40 µl of dissolved S-NHS were added to beads. The beads were sonicated for 3 min and nutated at low speed until visible clumps disappeared. The beads were rinsed in phosphate-buffered saline (PBS, pH 7.4) buffer in 800 µl total volume and reacted with 200 µl of 0.4 mg ml $^{-1}$  antibody. After shaking the mixture for 30 min, the beads were passivated by adding 10 mg ml $^{-1}$  bovine serum albumin (BSA) for 2h, washed in PBS three times and stored in PBS supplemented with 0.1% sodium azide and 0.5 mg ml $^{-1}$  BSA at 4 °C.

Sample preparation. Cy5-labelled axonemes were flowed into the chamber in dynein lysis buffer (DLB) buffer (30 mM HEPES pH7.2, 2 mM MgCl<sub>2</sub>, 1 mM EDTA, 10% glycerol). To determine the polarity of the axonemes, TMR-labelled DHA-GST-Dyn $_{\rm 331kD}$  was flowed into the chamber with 1 mM ATP in DLBC buffer (DLB supplemented with 1 mg ml $^{-1}$  casein and 2 mM dithiothreitol (DTT)). After waiting for 5 min to allow dynein to accumulate at the MT minus-end, the chamber was washed three times with 30 µl DLBC. GFP-tagged S. cerevisiae dynein was mixed with anti-GFP-coated beads for 10 min on ice. For DNA-tethered optical trapping experiments, monomeric S. cerevisiae dynein labelled with a DNA tether was incubated with streptavidin-coated polystyrene beads (860 nm in diameter, Spherotech) for 5 min on ice. The motor–bead mixture was introduced into the chamber along with 1 mM ATP and an oxygen scavenger mixture (35 mg ml $^{-1}$  protocatechuic acid (PCA) and 2.5 mM protocatechuate-3,4-dioxygenase (PCD)).

For trapping experiments with mammalian dynein–dynactin, DDB complexes were assembled by mixing  $1\,\mu l$  of  $1.2\,mg\,ml^{-1}$  dynein with  $1\,\mu l$  of  $1.6\,mg\,ml^{-1}$  dynactin, and  $1.5\,\mu l$  of  $3-4\,mg\,ml^{-1}$  cargo adaptor (BicD2N-GFP) in  $10\,\mu l$  dynein motility buffer (DMB: 30 mM HEPES pH7.0, 5 mM MgSO $_4$ , 1 mM EGTA, 1 mM TCEP (tris(2-carboxyethyl)phosphine) supplemented with 1 mg ml $^{-1}$  BSA. The complex was incubated on ice for 10 min. The complex assembly was incubated with anti-GFP-coated beads for 10 min on ice, diluted in DMB supplemented with 1.25 mg ml $^{-1}$  casein (DMB-C), 5 U ml $^{-1}$  of apyrase, 2.5 mM PCA and 50 nM PCD, and flowed into the chamber.

To ensure that more than 95% of the beads were driven by single dyneins, the motor to bead ratio was reduced until less than 30% of the beads walked along MTs in the presence of ATP. To test the motility of the dynein-driven beads in the absence of nucleotide, instead of 1 mM ATP,  $5\,\mathrm{U\,ml^{-1}}$  of apyrase was added to the motor–bead mixture to deplete the residual ATP in the chamber.

MT gliding assays. To polymerize MTs, unlabelled and Cy5-labelled pig tubulin were mixed in BRB80 buffer (80 mM PIPES pH 6.8, 1 mM MgCl<sub>2</sub>, 1 mM EGTA,

1 mM DTT) supplemented with the polymerization mixture (2 mM GTP, 20% dimethyl sulfoxide (DMSO) in 2× BRB80). MTs were polymerized for 20 min at 37 °C, then 10  $\mu$ M taxol was added to the mixture and incubated for an additional 10 min at 37 °C. Excess tubulin was removed by pelleting and resuspending MTs at 20,000g for 12 min in BRB80 supplemented with 10  $\mu$ M taxol. MTs were stored at room temperature in the dark.

To exert forces on MTs during gliding motility, beads were densely coated with a construct that contained dynein MTBD and part of the stalk coiled-coil fused to monomeric seryl-tRNA synthetase (GFP-SRS\_85,82-MTBD)  $^{30}$ . A 2  $\mu$ l volume of 5  $\mu$ M GFP-SRS\_85,82-MTBD was incubated with 1  $\mu$ l of 4% vol/wt bead solution for 5 min. Excess protein was removed by the addition of 1 ml DLB, and pelleting and resuspending the beads in 5  $\mu$ l DLB. DHA-GST-Dyn\_331kD was labelled with biotin at the N terminus and fixed onto the glass surface through a BSA-biotin and streptavidin linkage. The sample was washed with DLB, and  $10\,\mu$ l of 0.1 mg ml $^{-1}$  Cy5 MTs were introduced to the chamber in the presence of  $10\,\mu$ M taxol. After 2 min incubation,  $40\,\mu$ l of 20 mg ml $^{-1}$  beads were introduced to the chamber in DLB supplemented with  $20\,\mu$ M TR,  $10\,\mu$ M taxol, oxygen scavenger mixture (2.5 mM PCA and 50 nM PCD) and the ATP regeneration mixture (2 mM phosphoenolpyruvate and  $0.42\,\text{mM}$  pyruvate kinase).

Optical trapping assays. All trapping experiments were performed on a fully automated optical trap that was custom-built in an acoustically isolated and temperature-controlled (±0.1 °C) room around the body of a Nikon Ti-E inverted microscope<sup>11</sup>. Beads were trapped using a 2W 1,064 nm laser (Coherent). The trapping beam was focused on the image plane using a ×100 1.49 numerical aperture (NA) apochromat oil-immersion objective (Nikon). Cy5-labelled axonemes or MTs were excited using a 632 nm HeNe laser (Melles Griot) and imaged via a monochrome charge-coupled device camera (The Imaging Source). MTs were moved to the centre of the field of view using a locking XY stage (M-687, Physik Instrumente). A pair of perpendicular acousto-optical deflectors (AA Optoelectronic) were placed in a plane conjugate to the back focal plane of the objective to steer the trap. The laser power was adjusted with a half-wave plate on a motorized rotary mount (New Focus). Beads were lowered on the axonemes using a piezo flexure objective scanner (P-721 PIFOC, Physik Instrumente). The bead position relative to the centre of the trap was determined by imaging the back focal plane of a 1.4 NA oil immersion condenser (Nikon) on a position-sensitive detector (First Sensor). Calibration of the detector response was performed by raster-scanning the laser across a trapped bead with the acousto-optical deflector12. The power spectrum of a trapped bead position was fit to a lorentzian to obtain the trap stiffness.

Freely diffusing monodisperse beads were trapped and lowered onto a surface-immobilized Cy5-labelled axoneme oriented parallel to the PSD horizontal axis. To perform constant force assays in the presence of ATP, force-feedback control was activated after the beads moved 40 nm away from the trap centre. In the absence of ATP, MT polarity was determined by allowing TMR-labelled dynein to walk on axonemes for 5 min and accumulate at the minus-end before washing the assay solution and replacing it with the bead-motor mixture and apyrase. A trapped bead was lowered onto an axoneme and briefly released and trapped until it bound to an MT. Force feedback was applied in the forward or backward directions. The magnitude of the applied force was adjusted by changing the laser power while keeping the bead-trap separation at 100 nm. The bead position was acquired at 5kHz and the trap position was updated at 100 Hz to keep the bead-trap separation constant. The trap stiffness was set to 37.5 fN nm<sup>-1</sup>. The thermal relaxation of the bead (300 Hz) was taken to be roughly equal to the corner frequency of the trap.

Force oscillation experiments were performed using the force-feedbackcontrolled trap. The applied force was alternated periodically in a square-wave pattern at 2.5 Hz, two order of magnitude slower than the thermal relaxation of the trapped bead (300 Hz). To enable more rapid and accurate switching between the assisting and hindering forces, we commanded the trap to move by an experimentally estimated offset every time it switched between the forward and backward feedback setpoints. This compensated for the free rotation of the bead, which results in a movement without a net force exerted on the bead. This 'dead' region corresponds to the 250-500 nm difference between bead positions under the forward and backward pull of the trap, despite the motor remaining attached to the MT. For experiments with zero  $\bar{F}$  on the bead, the bead–trap separation was kept constant at 100 nm and the trap stiffness was adjusted to apply the desired forces on the bead. In experiments where  $\Delta F$  was kept constant, force bias was provided by using different trap-bead separation distances when the bead was pulled towards the plus- and minus-ends of an MT. Over 90% of the applied force was along the long axis of the MT, whereas the short axis deviated from the trap centre negligibly during data collection.

For release rate measurements, beads that were sparsely coated with tail-truncated dynein monomers (GFP-Dyn $_{\rm 331kD}$ -DHA) $^{16}$  were placed onto an axoneme and oscillated with a period of 0.7 s between two positions ( $\pm 100\,\mathrm{nm}$ ). MT polarity was determined using TMR-labelled dynein, as described above. The bead position was fitted to a step-finding algorithm $^{12}$  to detect individual release events. The bead to motor ratio was adjusted such that more than 80% of release events occurred in a single step. Release events occurring in more than a single step and dwells shorter than 3 ms were discarded from the analysis. Release data were sorted and binned by force. The cumulative distribution of each bin was fitted to a double exponential

decay to determine the fast  $(k_1)$  and slow  $(k_2)$  release rates. The double exponential decay fit was statistically justified using the F-test.

In the MT gliding assays, the surface density of dynein was sufficient to glide MTs on a straight path for several micrometres throughout force application. Freely diffusing polystyrene beads were lowered to a gliding MT between 4 and  $10\,\mu m$  in length. These beads were tightly bound to the MT as soon as they came into contact with each other. After MT binding, the force-feedback-controlled trap was engaged and the bead was pulled along the MT long axis back and forth at 2.5 Hz. The beads remained firmly attached to the MTs during force oscillations. The external force did not alter the direction of gliding motility. The bead–trap separation was kept at  $100\,nm$  and forces on the bead were adjusted by altering the trap stiffness.

Data analysis. Traces were recorded at 5 kHz, downsampled to 500 Hz and visualized using custom software written in MATLAB. Trajectories containing instantaneous jumps greater than 40 nm were excluded from the data analysis because this distance exceeds the maximum size of the steps that dynein takes. For the force–velocity measurements, the minimum accepted run time was 200 ms. The velocity was calculated by dividing the total distance travelled by the elapsed time during force application. Power was calculated by multiplying the average force on the bead and the velocity of the motor movement. For step size analysis, trajectories were downsampled to 100 Hz and fitted to a step-finding algorithm using the Schwartz information criterion<sup>11</sup>. The step size versus force graphs in Extended Data Figs. 3c and 4c were interpolated using an exponential function. The step size was set to zero at 0 pN in no ATP and at 3.1 pN in 1 mM ATP.

**Reporting Summary.** Further information on research design is available in the Nature Research Reporting Summary linked to this article.

#### Data availability

The data represented in Figs. 1–4 and Extended Data Figs. 2, 3, 4 and 6 are available as source data in the Supplementary Information. All other data that support the plots within this paper and other findings of this study are available from the corresponding author upon reasonable request. Yeast strains used in this study are available from the corresponding author upon request.

#### Code availability

Software and code used in this study are available from the corresponding author upon request.

#### References

- Zhang, K. et al. Cryo-EM reveals how human cytoplasmic dynein is auto-inhibited and activated. Cell 169, 1303–1314 (2017).
- Schlager, M. A., Hoang, H. T., Urnavicius, L., Bullock, S. L. & Carter, A. P. In vitro reconstitution of a highly processive recombinant human dynein complex. EMBO J. 33, 1855–1868 (2014).
- Urnavicius, L. et al. Cryo-EM shows how dynactin recruits two dyneins for faster movement. *Nature* 554, 202–206 (2018).
- 34. King, S. J. & Schroer, T. A. Dynactin increases the processivity of the cytoplasmic dynein motor. *Nat. Cell Biol.* **2**, 20–24 (2000).
- Carter, A. P. et al. Structure and functional role of dynein's microtubulebinding domain. Science 322, 1691–1695 (2008).

#### Acknowledgements

We thank L. Ferro, M. ElShenawy and N. Hendel for their help in the initiation of this project, and the rest of the Yildiz Laboratory members for helpful discussions and technical assistance. This work was funded by grants from the NIH (GM094522) and NSF (MCB-1055017, MCB-1617028) to A.Y. and an NSF Graduate Research Fellowship (DGE 11064000) to V.B.

#### **Author contributions**

V.B. built the microscope and initiated the oscillation trap experiments. Y.E. and S.C. prepared the protein and antibody-coated beads. Y.E. performed single-molecule experiments and analysed the data. A.Y. and Y.E. wrote the manuscript. A.Y. supervised the project.

#### **Competing interests**

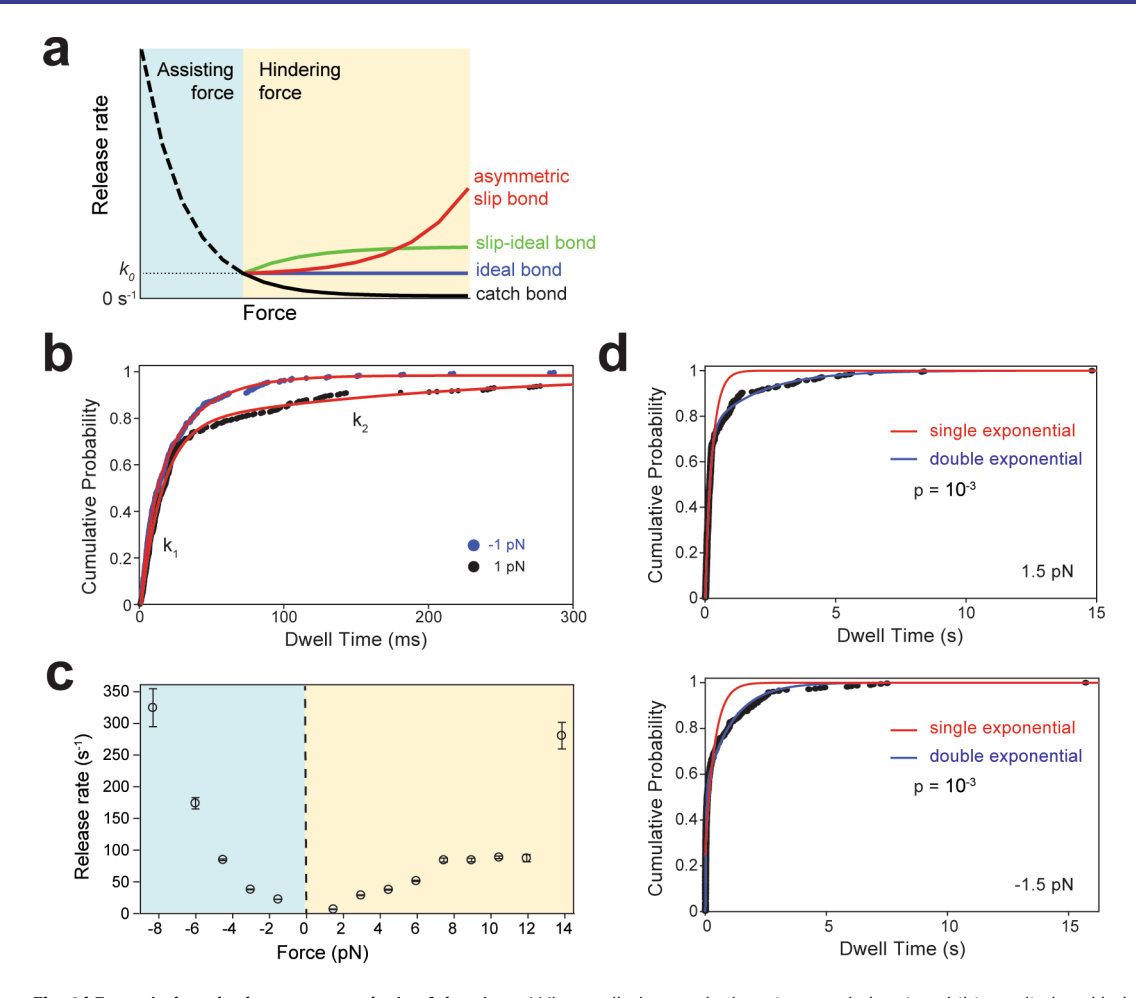
The authors declare no competing interests.

#### Additional information

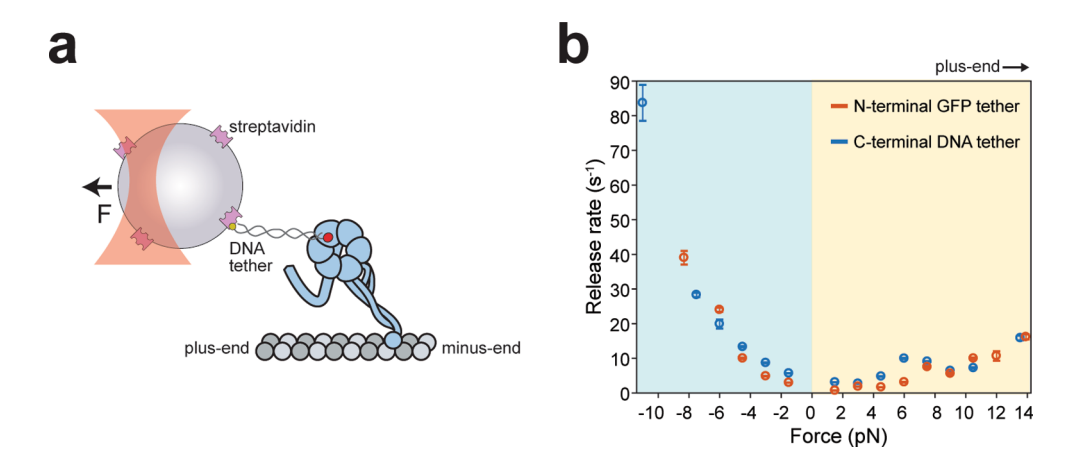
**Extended data** is available for this paper at https://doi.org/10.1038/s41567-019-0757-4. **Supplementary information** is available for this paper at https://doi.org/10.1038/s41567-019-0757-4.

Correspondence and requests for materials should be addressed to A.Y.

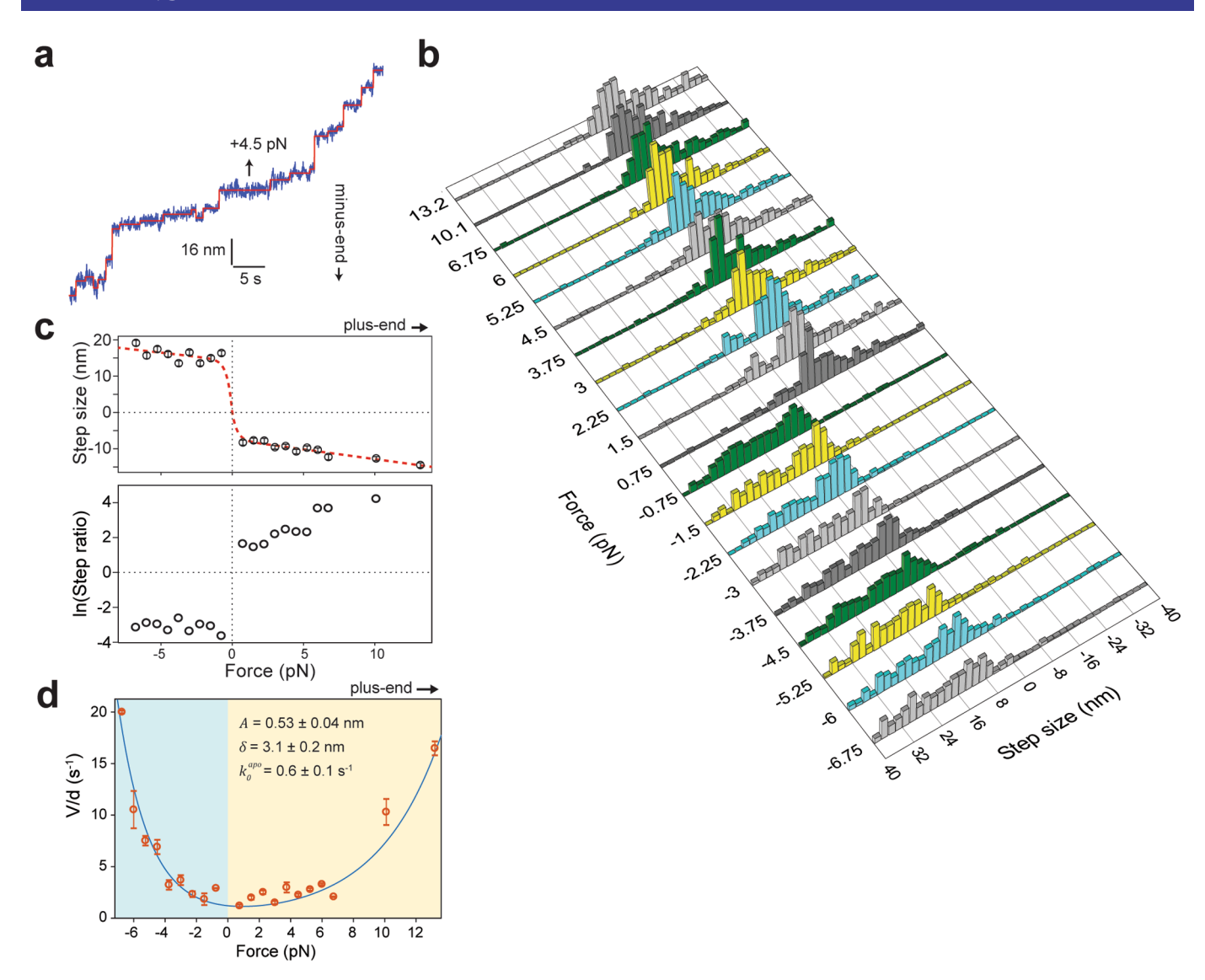
Reprints and permissions information is available at www.nature.com/reprints.



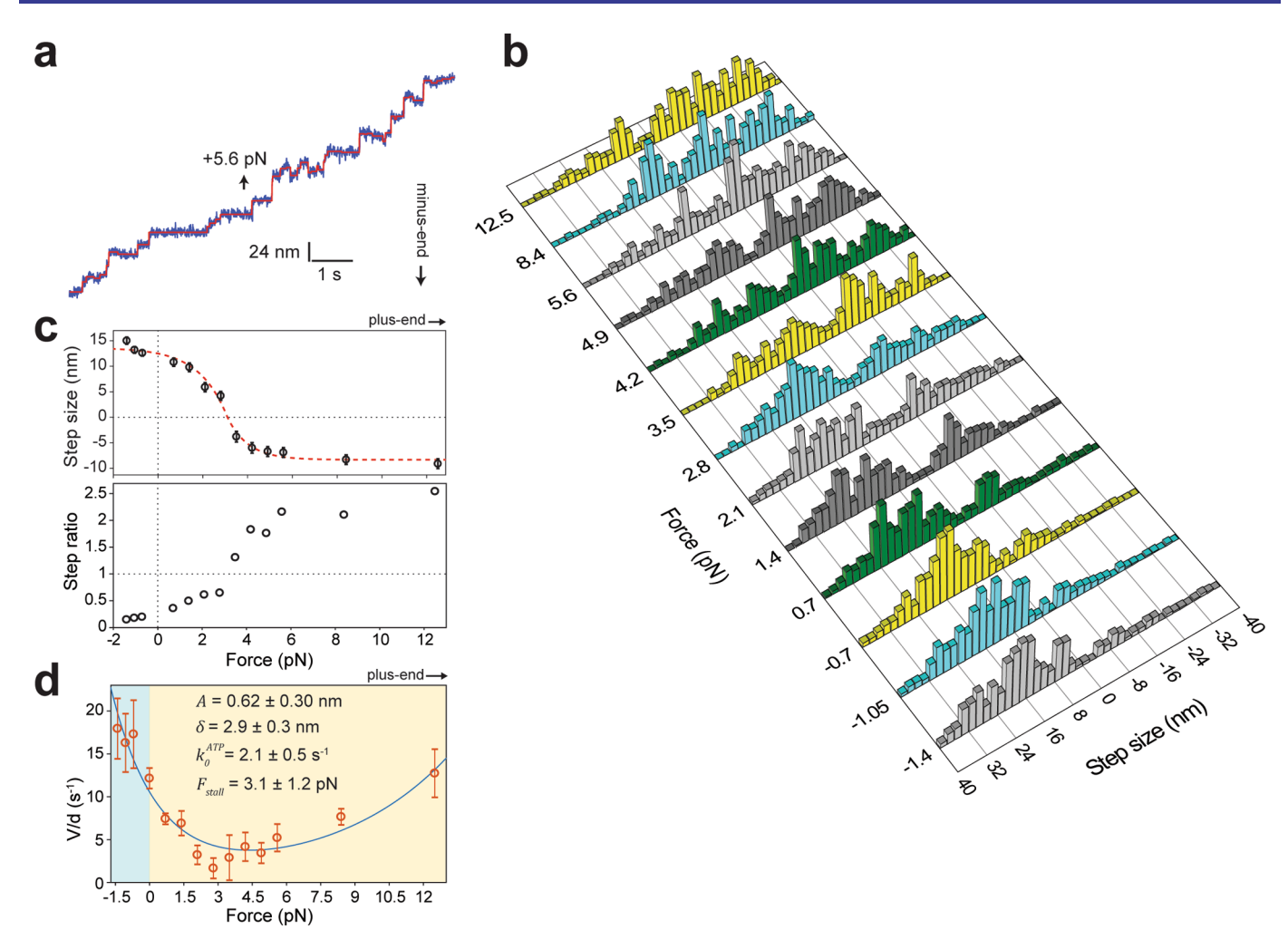
**Extended Data Fig. 1** Force-induced release rate analysis of dynein. **a.** When pulled towards the minus-end, dynein exhibits a slip bond behavior with an MT, in which the release rate increases exponentially by assisting force (black dashed curve). In the hindering direction, possible force-detachment kinetics of slip, slip-ideal, ideal and catch bond behavior are shown for comparison (solid curves). **b.** Cumulative distributions of dynein dwell time on an MT under a given force were fit to a double exponential decay (red curves) to calculate fast ( $k_1$ ) and slow ( $k_2$ ) release rates from MT. n = 504 for 1pN and 512 for -1 pN. **c.**  $k_1$  of dynein from MT (mean  $\pm$  s.e.m.; n 270, 243, 479, 407, 385, 354, 487, 461, 380, 260, 208, 325, 137, 325 from left to right). This rate likely represents a weak interaction between dynein and tubulin. Similar to  $k_2$  (Fig. 1c),  $k_1$  increases with force in both directions. **d**. Comparison of the single and double exponential fit to example cumulative distributions of dynein dwell time. p values are calculated using F-test.



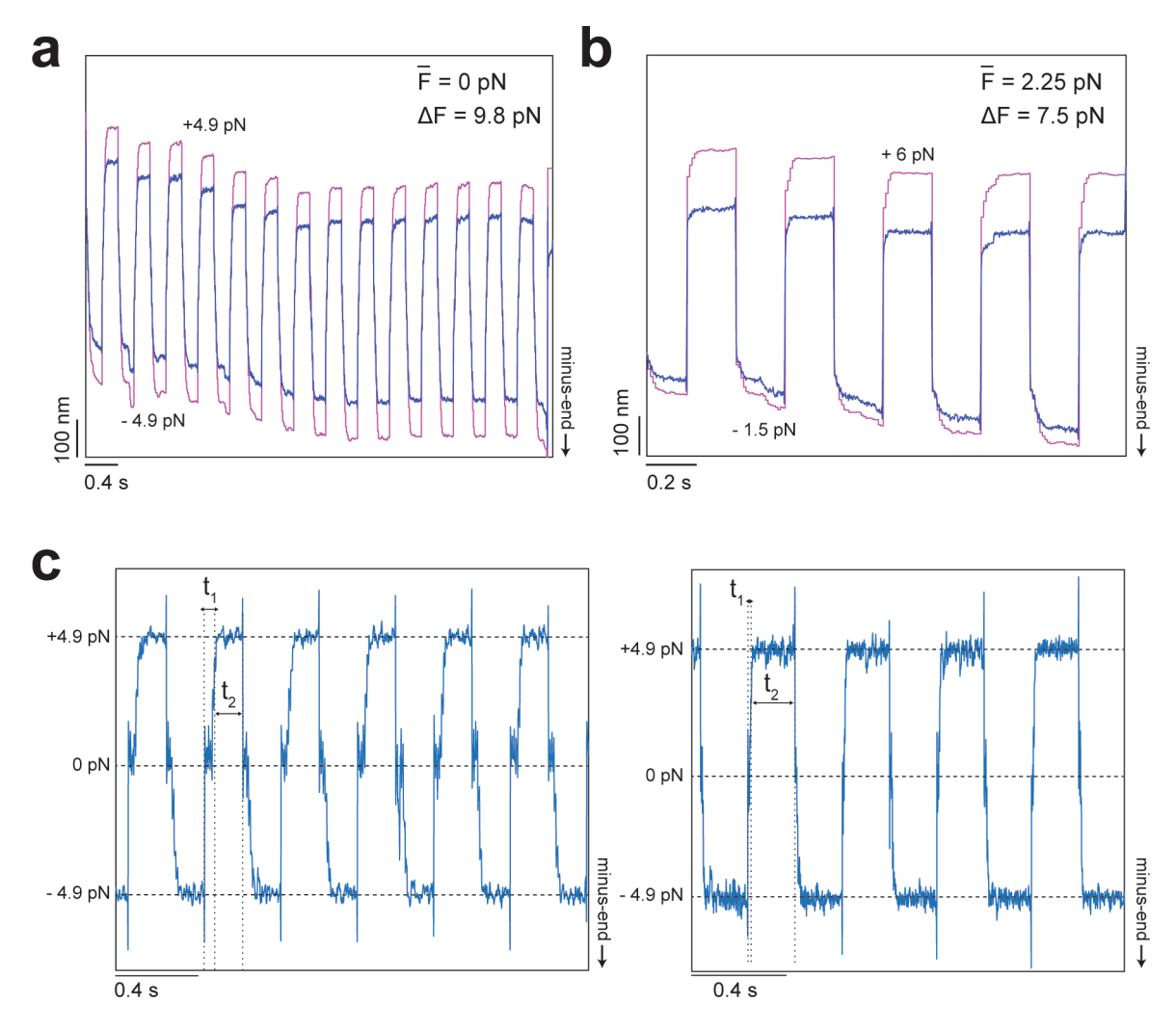
Extended Data Fig. 2 | Measurement of force-detachment kinetics of dynein using a DNA-tethered optical trap. a. A tail truncated dynein monomer (GFP-Dyn<sub>33lkD</sub>-DHA) was labeled with a 74 bp DNA tether at its C-terminal DHA tag using the HaloTag chemistry. The DNA-labeled motor was attached to a bead via a biotin-streptavidin linkage. b. MT release rates of dynein monomers pulled from the C-terminal AAA ring via a DNA tether (blue, mean  $\pm$  s.e.m.; from left to right n = 534, 661, 251, 973, 1074, 1742, 3216, 1423, 1003, 984, 792, 501, 310, 240 from three technical replicates). MT release rates of dynein monomers pulled from the N-terminal linker via the GFP-antibody (red, Fig. 1c) are shown for comparison.



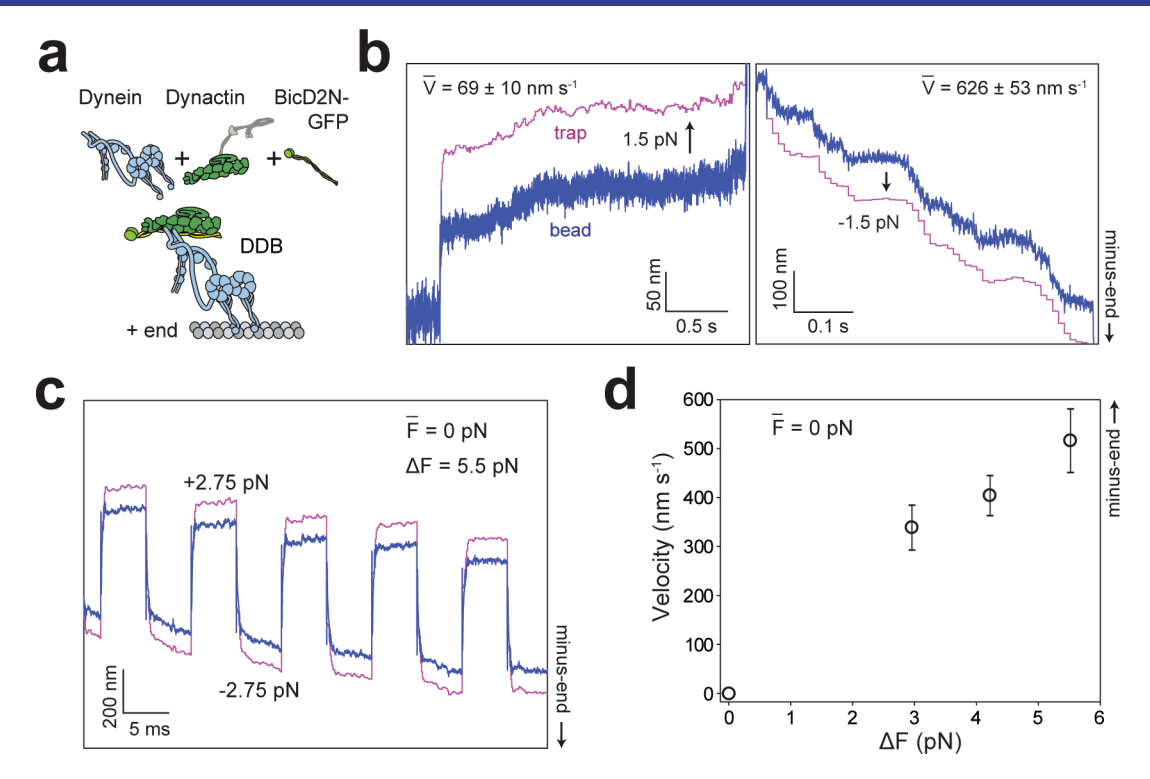
**Extended Data Fig. 3** | Force-induced stepping of dynein in the absence of ATP. a. Example trajectory of a bead driven by single full-length dynein at 4.5 pN hindering force (blue) in the absence of ATP. Red horizontal lines represent a fit with a step finding algorithm (see Methods). **b.** Step size distribution of dynein under assisting and hindering forces in the absence of ATP (n= 214, 207, 204, 203, 266, 316, 308, 400, 211, 233, 247, 233, 202, 204, 238, 205, 226, 203, 208, 265 steps from hindering to assisting forces). **c.** (Top) The average step size of dynein under different forces. Positive steps are in the minus-end direction. Error bars represent s.e.m. The red dashed curve is an interpolation of the data to an exponential function. (Bottom) The ratio of steps taken in the plus-end direction to minus-end-direction. **d.** The ratio of the experimentally measured velocities (Fig. 2b) to the average step size (c) in the absence of ATP. The errors represent s.e.m. of velocity measurements (Fig. 2b). The blue curve represents a fit to equation 3. The errors of the derived parameters are s.e. of the fit.



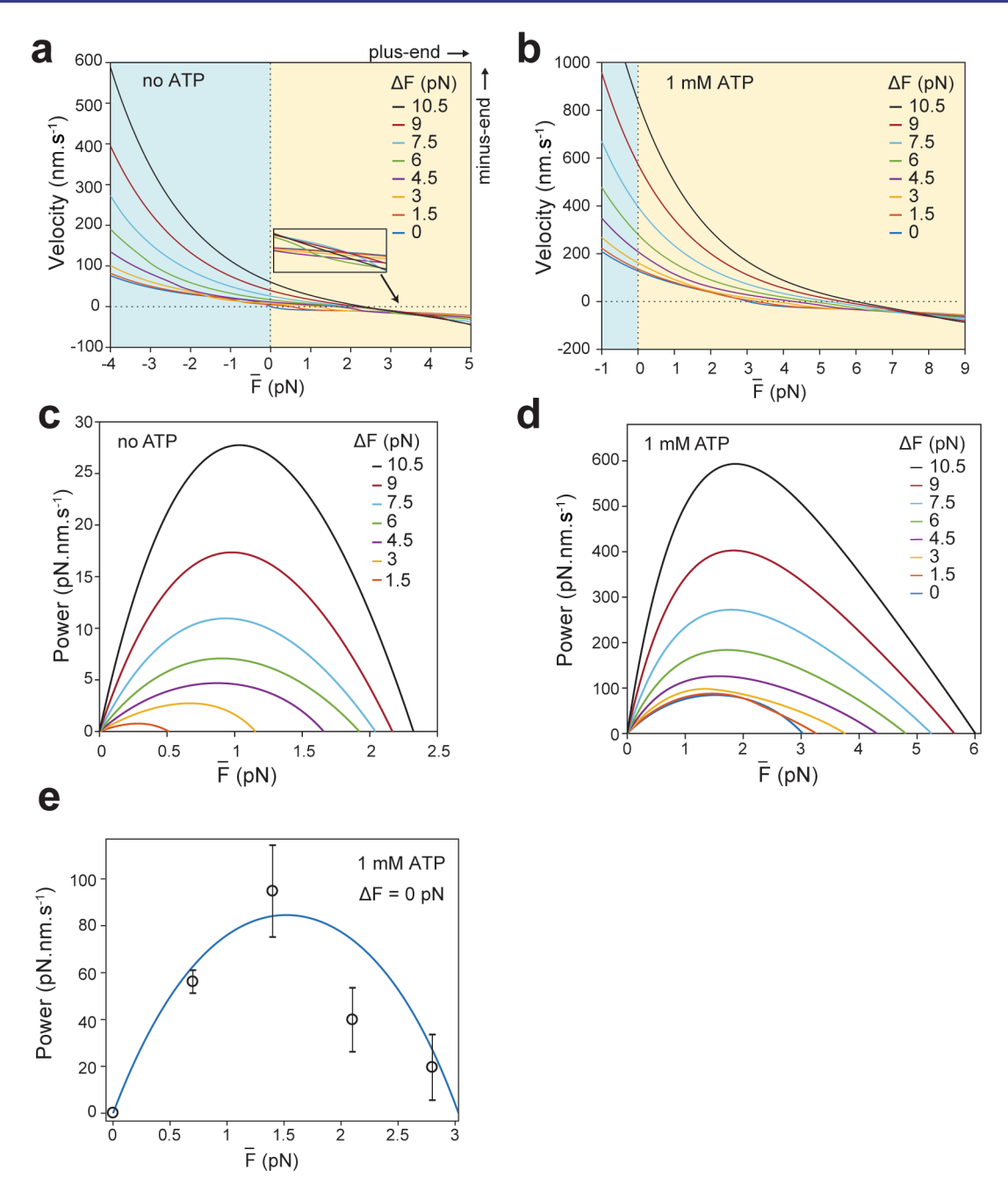
**Extended Data Fig. 4 | Force-induced stepping of dynein in 1 mM ATP. a.** Example trajectory of a bead driven by single full-length dynein at 5.6 pN hindering force (blue). Red horizontal lines represent a fit with a step finding algorithm. **b.** Step size distribution of dynein under assisting and hindering forces (n = 447, 428, 492, 430, 440, 460, 442, 291, 314, 381, 335, 298, 340 steps from hindering to assisting forces).**c.**(Top) The average step size of dynein under different forces. Error bars represent s.e.m. The red dashed curve is an interpolation of the data to an exponential function. (Bottom) The ratio of steps taken in the plus-end direction to minus-end-direction.**d.**The ratio of the experimentally measured velocities (Fig. 2c) to the average step sizes (c) in 1 mM ATP. The errors represent s.e.m. of velocity measurements (Fig. 2c). The blue curve represents a fit to equation 5. The errors of the derived parameters are s.e. of the fit.



**Extended Data Fig. 5 | Example traces for nucleotide-free oscillations. a.** Example trajectory of a dynein-driven bead oscillated  $\pm$  4.9 pN in a square wave pattern without ATP. **b.** Example trajectory of a dynein-driven bead oscillated with  $\pm$  6 pN and  $\pm$  1.5 pN in a square wave pattern at 2.5 Hz. Even though dynein was pulled more strongly backward, it moved towards the MT minus-end in the absence of ATP. **c.** The bead position was subtracted from the trap position to determine the force exerted on the bead during force oscillations. Due to the thermal relaxation of the bead and the rotational freedom of the bead-motor linkage, the bead-trap separation reaches near zero when the bead is moved between forward and backward positions. To determine how force affects velocity, this "dead" period  $\pm$  1 is omitted from total elapsed time and  $\pm$  2 is taken as half period of oscillations. (Left) To switch between assiting and hindering forces, the trap was first moved 250 nm and then with proportional feedback-controlled increments every 10 ms until the desired force was reached. (Right) The trap was first moved 500 nm and then with feedback-controlled increments every 10 ms until the desired force was reached. An increase in this "overshoot" distance decreased  $\pm$ 1.



Extended Data Fig. 6 | Force oscillations facilitate ratcheting of mammalian dynein-dynactin towards the minus-end of MTs in the absence of ATP. a. The assembly of the mammalian dynein-dynactin-BicD2 (DDB) complex from human dynein, pig-brain dynactin and the N-terminal coiled-coil of mouse BicD2 (BicD2N, 1-400). BicD2N was fused with GFP at its C terminus for attachment of the complex to anti-GFP-coated beads. **b**. Example trajectories of DDB-driven beads pulled towards the MT plus- (left) and minus- (right) end under 1.5 pN force. The average velocities (mean  $\pm$  s.e.m.) were calculated from 44 (left) and 27 (right) trajectories. **c**. Example trajectory of a DDB-driven bead oscillated  $\pm$  2.75 pN in a square wave pattern at 10 Hz. Similar to beads driven by *S. cerevisiae* dynein, DDB processively drives the bead towards the MT minus-end. **d**. The velocity of DDB-driven beads increases with  $\Delta$ F in the absence of net force on the bead (mean  $\pm$  s.e.m.; from left to the right n = 25, 32, 26 from three technical replicates). In comparison, DDB ratcheted faster towards the MT minus-end than S. cerevisiae dynein.



**Extended Data Fig. 7 | Force fluctuations increase the power output of dynein towards the minus-end. a, b.** Estimated  $\bar{F} - V$  relationship under different  $\Delta F$  in the absence (**a**) and presence (**b**) of 1mM ATP. The model predicts that increasing  $\Delta F$  leads to faster minus-end directed velocities at  $\bar{F} = 0$  pN and higher average hindering forces to stall the bead movement. The inset in (**a**) shows that the curves do not intersect at the same point. **c, d.** Force oscillations increase the power output of dynein in the absence (**c**) and presence (**d**) of 1mM ATP. The power output of dynein at average hindering forces was calculated from the F-V relationship. **e.** Power output of dynein (black circles, mean  $\pm$  s.e.m.; n = 42, 56, 58, 47 from left to right) in 1mM ATP and in the absence of force fluctuations ( $\Delta F = 0$  pN). The blue curve corresponds to the 0 pN curve in **d**.



| Corresponding author(s):   | Ahmet Yildiz |
|----------------------------|--------------|
| Last updated by author(s): | Nov 7, 2019  |

# **Reporting Summary**

Nature Research wishes to improve the reproducibility of the work that we publish. This form provides structure for consistency and transparency in reporting. For further information on Nature Research policies, see Authors & Referees and the Editorial Policy Checklist.

| _ |      |     |    |    |   |
|---|------|-----|----|----|---|
| ۲ | · a. | ŀi٠ | ct | i۲ | c |

| For all statistical analy     | ses, confirm that the following items are present in the figure legend, table legend, main text, or Methods section.   |  |  |  |  |  |
|-------------------------------|--|--|--|--|--|--|
| n/a Confirmed                 |  |  |  |  |  |  |
| ☐ ☐ The exact sar             | The exact sample size ( $n$ ) for each experimental group/condition, given as a discrete number and unit of measurement  |  |  |  |  |  |
| A statement                   | A statement on whether measurements were taken from distinct samples or whether the same sample was measured repeatedly  |  |  |  |  |  |
| The statistica Only common    | al test(s) used AND whether they are one- or two-sided tests should be described solely by name; describe more complex techniques in the Methods section.  |  |  |  |  |  |
| A description                 | n of all covariates tested   |  |  |  |  |  |
| A description                 | A description of any assumptions or corrections, such as tests of normality and adjustment for multiple comparisons  |  |  |  |  |  |
| A full descrip                | tion of the statistical parameters including central tendency (e.g. means) or other basic estimates (e.g. regression coefficient) n (e.g. standard deviation) or associated estimates of uncertainty (e.g. confidence intervals) |  |  |  |  |  |
| For null hypo                 | othesis testing, the test statistic (e.g. $F$ , $t$ , $r$ ) with confidence intervals, effect sizes, degrees of freedom and $P$ value noted as exact values whenever suitable.   |  |  |  |  |  |
| For Bayesian                  | analysis, information on the choice of priors and Markov chain Monte Carlo settings  |  |  |  |  |  |
| For hierarchi                 | cal and complex designs, identification of the appropriate level for tests and full reporting of outcomes  |  |  |  |  |  |
| Estimates of                  | effect sizes (e.g. Cohen's $d$ , Pearson's $r$ ), indicating how they were calculated  |  |  |  |  |  |
| '                             | Our web collection on <u>statistics for biologists</u> contains articles on many of the points above.  |  |  |  |  |  |
| Software and                  | code   |  |  |  |  |  |
| Policy information abo        | out <u>availability of computer code</u>   |  |  |  |  |  |
| Data collection               | For hardware control of microscope: Labview 2017 For image acquisition: Andor Solis For Nikon Microscope Body Control: Ti Control 4.4.2  |  |  |  |  |  |
| Data analysis                 | For image handling: FIJI 1.0<br>For data analysis: MATLAB (R2017), Imagej (v.1.51r), Origin Pro 9.0  |  |  |  |  |  |
| For manuscripts utilizing cus | stom algorithms or software that are central to the research but not yet described in published literature, software must be made available to editors/reviewers.  |  |  |  |  |  |

We strongly encourage code deposition in a community repository (e.g. GitHub). See the Nature Research guidelines for submitting code & software for further information.

## Data

Policy information about availability of data

All manuscripts must include a data availability statement. This statement should provide the following information, where applicable:

- Accession codes, unique identifiers, or web links for publicly available datasets
- A list of figures that have associated raw data
- A description of any restrictions on data availability

Yeast strains, coding and the data that support the findings of this study are available from the corresponding author upon request.

| Field-specific reporting  |  |   |  |  |  |  |
|---|--|---|--|--|--|--|
| Please select the or  | Please select the one below that is the best fit for your research. If you are not sure, read the appropriate sections before making your selection. |   |  |  |  |  |
| ∑ Life sciences   | Life sciences Behavioural & social sciences Ecological, evolutionary & environmental sciences  |   |  |  |  |  |
| For a reference copy of t   | he document with   | all sections, see <u>nature.com/documents/nr-reporting-summary-flat.pdf</u>   |  |  |  |  |
| Life scier  | nces sti   | udy design  |  |  |  |  |
|   |  | points even when the disclosure is negative.  |  |  |  |  |
| Sample size   |  | ermined sample size used in the experimental design.  |  |  |  |  |
| Data exclusions   |  | ate experiments under optical trap, attachments that are shorter than 3 ms were excluded from analysis.   |  |  |  |  |
| Replication   |  | y and biochemical assays were reproduced from 3 replicates. o data were reproduced from at least 3 independent replicates.                                  |  |  |  |  |
| Randomization   | N/A  |   |  |  |  |  |
| Blinding  | N/A  |   |  |  |  |  |
| We require informatic system or method list  Materials & exp  n/a   Involved in th    Antibodies     Eukaryotic     Palaeontold     Animals an     Human reserved     Clinical data | on from authors led is relevant to cerimental s e study cell lines ogy d other organism earch participan   | n/a Involved in the study  ChIP-seq  Flow cytometry  MRI-based neuroimaging   |  |  |  |  |
| Antibodies  |  |   |  |  |  |  |
| Antibodies used   |  | Custom made anti-GFP antibodies (Covance Inc.) were purified by GFP affinity chromatography to be used in carboxyl latex beads (Life Technologies) coating. |  |  |  |  |
| Validation  | Ve   | Verified by EMSA assays.  |  |  |  |  |
| Eukaryotic c  | ell lines  |   |  |  |  |  |
| Policy information a  | about <u>cell lines</u>  |   |  |  |  |  |
| Cell line source(s)   | )  | S. cerevisiae strains and insect cells were used for protein purification.  |  |  |  |  |
| Authentication  |  | No authentication was used.   |  |  |  |  |

Cells were not tested for mycoplasma contamination.

Mycoplasma contamination

Commonly misidentified lines (See <u>ICLAC</u> register)

N/A